

MAXIMUM LIKELIHOOD ESTIMATOR FOR MAGNETO-ACOUSTIC LOCALISATION

Gilles Dassot[⊙], Roland Blanpain[⊙], Claude Jauffret[⊙]

[⊙] LETI (CEA - Technologies Avancées) DSYS
CEA/Grenoble - 17, rue des martyrs - 38054 Grenoble Cedex 9 - France

[⊙] GESSY
Université de Toulon et du Var - Bat. X - 83130 La Garde - France
First author's e-mail: Gilles.Dassot@cea.fr

ABSTRACT

This paper is devoted to the localization of magneto-acoustic sources moving in a straight line at a constant speed. Our technique is based on the association of narrow band acoustic signals and magnetostatic measurements. First of all, we describe features that make possible the association of magnetic and acoustic data, secondly, we show that positioning accuracy is much improved by this association. In this paper we focus on solving the problem with as few sensors as possible. A geometric discussion of identifiability is proposed, as well as a Batch Maximum Likelihood estimator whose covariance matrix asymptotically achieves Cramèr Rao Lower Bounds (CRLB).

1. INTRODUCTION

In this paper we present a new localization technique for magneto-acoustic sources when only few spatially distributed sensors are available. After a comparison of narrow band acoustic Doppler and Magnetic Anomaly Detection (MAD), we discuss the localization problem identifiability depending on the sensor geometrical layout. The Maximum Likelihood estimator is then proposed and Monte Carlo simulation results are compared with theoretical CRLB.

2. COMPARISON OF ACOUSTIC DOPPLER AND MAGNETOSTATIC TECHNIQUES

We briefly recall the principles governing acoustic Doppler and Magnetostatic detection. A more detailed discussion may be found in [1]. We first underline two points of importance:

- we assume the source moving in a straight line at a constant velocity, and sensors and the speed vector being coplanar,
- both signals are signatures: the informative content of measured signals is actually due to the relative motion between sensor and target.

2.1. Acoustic Doppler Shifts

Acoustic emissions $s(t)$ undergo Doppler shifts due to the relative motion of the emitter and the receiver. In the case of narrow band signals, it is possible to extract frequency lines exhibiting such shifts [2]. Using notations of figure 1, the following equation shows localization parameters in the received frequency expression:

$$f = f_0 \left/ \left(1 + \frac{V}{C} \sin \theta \right) \right. \quad (1)$$

where f_0 denotes the emitted centre frequency and C the sound velocity.

2.2. Magnetic Anomaly Detection physical basis and estimation

Ferromagnetic objects are surrounded by a magnetostatic field and behave as magnetic dipoles provided that they are far enough from sensors. Such sensors measure the vector perturbation \mathbf{B} due to this field in the earth field:

$$\mathbf{B} = \frac{\mu_0}{4\pi r^5} \left[3\mathbf{xx}^T - r^2\mathbf{I} \right] \mathbf{M} \quad (2)$$

where \mathbf{M} denotes the dipolar moment, μ_0 is the air permittivity and \mathbf{x} denotes the source-to-sensor vector.

With a good approximation the signature of a constant speed source may be decomposed on an orthogonal Anderson basis governed by a set of two parameters $\{E/V, D/V\}$ (cf. figure 1) [3]. It is thereafter possible to perform a multidimensional matched filter on these signals yielding an estimate of the former set of parameters [3]. A specific difficulty of this technique is that estimates are only available shortly before the CPA.

We underline that D/V is unsigned and must be strictly considered as a distance. On the contrary E/V is signed

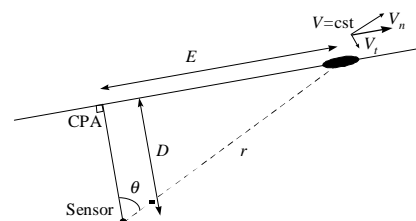


Figure 1. Illustration of the geometry with one sensor.

with respect to the orientated trajectory, its origin is usually taken at the CPA and it has time dimension.

3. ONE MEASUREMENT SITE LAYOUT

In this part we consider that a single measurement site performs both the acoustic and the magnetic detection as well as parameter extraction. The geometry is shown on figure 1. Measured parameters are thus $\mathbf{z}=[E/V, D/V, f]^T$, but some of them may not be available depending on the input Signal to Noise Ratios on $s(t)$ and $\mathbf{B}(t)$.

3.1. Identifiability considerations and CRLB

None of these sensors can achieve angular information, therefore the set of possible source location is a circle at best. If only magnetic parameters are available, the scaling factor of velocity in E/V and D/V yields an infinity of concentric circles.

If acoustic information can also be extracted, the set of possible source location reduces to one circle. In that case the instant of doubling the CPA t_{cpa} , its distance to the sensor D_{cpa} and the source velocity V are identifiable. The unknown center frequency f_0 should also be added to the final state vector, namely $\mathbf{x}=[t_{cpa}, D_{cpa}, V, f_0]^T$. Some geometrical considerations yields the following equation for noise free measurements:

$$\begin{aligned} E/V &= h_1(\mathbf{x}, t) = t - t_{cpa} \\ D/V &= h_2(\mathbf{x}, t) = D_{cpa}/V \\ f &= h_3(\mathbf{x}, t) = \frac{f_0}{1 + \frac{V^2(t-t_{cpa})}{C\sqrt{V^2(t-t_{cpa})^2 + D_{cpa}^2}}} \end{aligned} \quad (3)$$

If only acoustic parameters are available, local identifiability of \mathbf{x} may be established through the calculation of Cramèr Rao Lower Bound (CRLB) [5].

The CRLB is known to be the smallest covariance that any unbiased estimator of \mathbf{x} can achieved. It is calculated as the inverse of the Fisher Information Matrix (FIM), where:

$$\text{FIM} = -E \left[\frac{d^2}{d^2 \mathbf{x}} \ln \Lambda_{\mathbf{z}}(\mathbf{x}) \right] = -E \left[\frac{d^2}{d^2 \mathbf{x}} \ln p(\mathbf{z}|\mathbf{x}) \right] \quad (4)$$

where $\Lambda_{\mathbf{z}}(\mathbf{x})$ is the Likelihood of the set of measurements \mathbf{z} given \mathbf{x} .

In [5] the invertibility of the FIM is shown to be sufficient for local identifiability. Plots of CRLB for acoustic only measurements are drawn in black on figure 2.

Assuming the measurement noises $w_i(t_k)$ to be independent, normal and zero-mean distributed, the CRLB for $3K$ simultaneous measurements is finally:

$$\text{CRLB} = \left[\sum_{k=1}^K \sum_{m=1}^3 \left(\frac{dh_m(\mathbf{x}, t_k)}{d\mathbf{x}} \right)^T \frac{dh_m(\mathbf{x}, t_k)}{d\mathbf{x}} / \sigma_{k,m}^2 \right]^{-1} \quad (5)$$

As said before, magnetic parameters are only extracted with a good reliability after the CPA. Consequences of this are easily seen on figure 2, where the CPA is reached at 500 seconds. At this point, CRLB are drastically

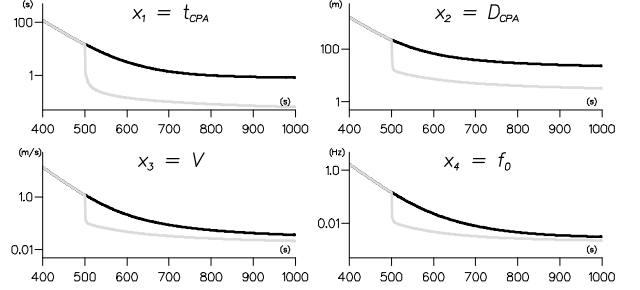


Figure 2. CRLB for one measurement site layout. Acoustic only in black, acoustic and magnetic in grey. The CPA is reached at 500sec. The source is moving at 10m/s, CPA distance is 1.5km, centre frequency is 200Hz. Log scale is used on vertical axis. Input standard deviations are $\sigma_{k,E/V}=1.0$, $\sigma_{k,D/V}=0.5$ for $t_k > 500$ and $\sigma=0.05$. improved.

3.2. Monte-Carlo Simulations

An efficient estimator is the Maximum Likelihood estimator, which maximizes $\Lambda_{\mathbf{z}}$ over the parameter space. Under gaussian assumption, a classical result is that maximizing the Likelihood yields the same estimate as minimizing an equivalent Least Square problem, namely:

$$\hat{\mathbf{x}} = \underset{\mathbf{x}}{\text{Argmin}} \left(\sum_{k=1}^K \sum_{m=1}^3 \frac{(z_m(t_k) - h_m(\mathbf{x}, t_k))^T}{(z_m(t_k) - h_m(\mathbf{x}, t_k)) / \sigma_{k,m}^2} \right) \quad (6)$$

An powerful algorithm for solving this problem is the Levenberg-Marquardt algorithm that realizes a trade-off between steepest descent and Gauss-Newton methods. Monte Carlo simulations are shown on figure 3.

A classical approximation in SONAR field is to use the first order Taylor expansion for h_3 in (3):

$$f \approx h_3'(\mathbf{x}, t) = f_0 \left(1 - \frac{V^2(t-t_{cpa})}{C\sqrt{V^2(t-t_{cpa})^2 + D_{cpa}^2}} \right) \quad (7)$$

Monte-Carlo simulations were also conducted in this case. It is shown in Table 1 that this approximation yields bias on f of the order of the corresponding standard deviation.

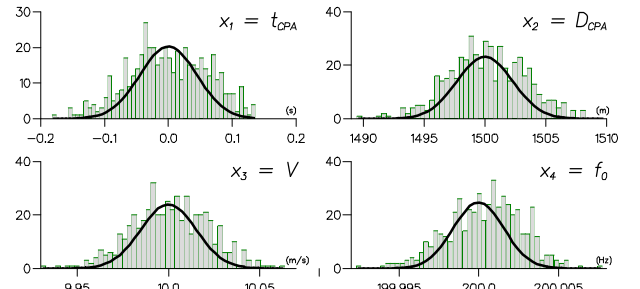


Figure 3. 500 Monte-Carlo simulations of the problem described in the caption of Figure 2 are conducted with Levenberg-Marquardt algorithm.

Table 1. Effects of first order Taylor expansion in h_3/h_3' on Monte-Carlo simulation results.

| | \mathbf{x}_{true} | $\hat{\mathbf{x}} - \mathbf{x}_{true}$ | $\hat{\mathbf{x}}' - \mathbf{x}_{true}$ | σ_{CRLB} | σ | σ' |
|-----------|---------------------|--|---|----------------------|----------------------|--|
| t_{cpa} | 0. | $-2.79 \cdot 10^{-3}$ | $-7.69 \cdot 10^{-3}$ | $6.31 \cdot 10^{-2}$ | $6.17 \cdot 10^{-2}$ | $6.33 \cdot 10^{-2}$ |
| D_{cpa} | 1500. | $1.80 \cdot 10^{-3}$ | $-4.40 \cdot 10^{-2}$ | 3.223 | 3.148 | 3.092 |
| V | 10. | $-1.35 \cdot 10^{-4}$ | $-3.97 \cdot 10^{-4}$ | $2.13 \cdot 10^{-2}$ | $2.09 \cdot 10^{-2}$ | $2.06 \cdot 10^{-2}$ |
| f_0 | 200. | $2.56 \cdot 10^{-4}$ | $5.56 \cdot 10^{-3}$ | $2.23 \cdot 10^{-3}$ | $2.30 \cdot 10^{-3}$ | $2.18 \cdot 10^{-3}$ |

4. MULTIPLE MEASUREMENT SITE LAYOUT

4.1. Identifiability considerations

In this case a small number (2 or 3) of distributed sensor sites are available. Each site allows extraction of either acoustic or magnetic or both parameters. In any case two distributed sensors orient the plane and the source location is identifiable except for some countable ghost solutions. Cartesian coordinates may be used for the state vector and the straight line of constant speed hypothesis allows to take this vector at some reference time. f_0 should also be added to the state vector and finally:

$$\mathbf{x} = [x_{tref} \quad y_{tref} \quad \dot{x} \quad \dot{y} \quad f_0]^T \quad (8)$$

Given two measurement sites, the source trajectory is tangent to two sensor-centered circles. As shown on figure 4, four solutions exist. Gray trajectories correspond to the same velocity V_a and black trajectories correspond to an other velocity V_b since points of tangency are not equally spaced. Solutions V_x and V_x' can not be discriminated because the scene is symmetrical with respect to sensor 1-to-sensor 2 axis. We recall indeed that

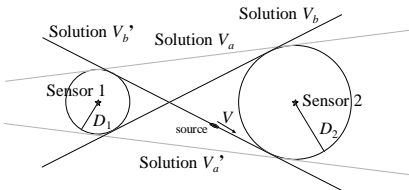


Figure 5. Ghost solutions with two measurement sites.

D/V is an unsigned parameter.

If only magnetic sensors are used, solutions V_a and V_b can not be discriminated neither, because of the scaling factor $1/V$ in the measured parameters. Four ghost solutions remain in this case. If at least one of the two is an acoustic sensor, solutions V_a and V_b can be discriminated and only two ghost solutions remain: either V_a and V_a' or V_b and V_b' .

If three or more unaligned sensors of any type are available, the source location is fully identifiable since symmetrical axis does not exist anymore and since confusion between V_a and V_b is no more possible either.

Two remarkable configurations shown on figure 5 should

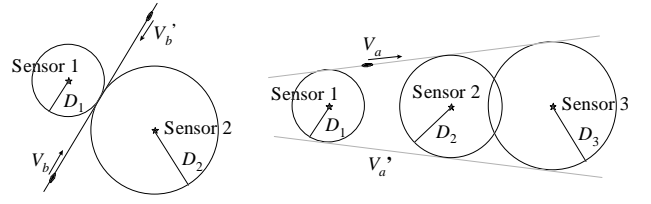


Figure 4. Remarkable configurations and associated ghost solutions.

be handled separately. If two sensors are used and their CPA time are equal, only one trajectory is possible but its orientation is unknown. If three or more sensors are on the same line, two ghost solutions remain because the symmetrical axis is not broken by the third sensor.

4.2. Cramèr Rao Lower Bounds

The following equation is established for a given site i where both acoustic and magnetic measurements are available. An other site j with the same kind of measurement equations should be used to ensure identifiability. These equations are based on geometrical facts and may be easily calculated. Noise free measurements are assumed in equation (9).

$$\begin{aligned} \left(\frac{E}{V}\right)_i &= \text{sign}_{t,i} \cdot \frac{\sqrt{(x_t - x_{cpa,i})^2 + (y_t - y_{cpa,i})^2}}{\sqrt{\dot{x}^2 + \dot{y}^2}} \\ \left(\frac{D}{V}\right)_i &= \frac{\sqrt{(x_{s,i} - x_{cpa,i})^2 + (y_{s,i} - y_{cpa,i})^2}}{\sqrt{\dot{x}^2 + \dot{y}^2}} \\ f_i &= \frac{f_0}{1 + \frac{1}{C} \frac{(x_t - x_{s,i})\dot{x} + (y_t - y_{s,i})\dot{y}}{\sqrt{(x_t - x_{s,i})^2 + (y_t - y_{s,i})^2}}} \end{aligned} \quad (9)$$

$$\begin{cases} x_t = x_{tref} + (t_k - t_{ref})\dot{x} \\ x_{CPA,i} = x_{C,i} + \frac{(x_{tref} - x_{C,i})\dot{y}^2 - (y_{tref} - y_{C,i})\dot{x}\dot{y}}{\dot{x}^2 + \dot{y}^2} \\ \text{sign}_{t,i} = \text{sign}(x_t - x_{CPA,i}) \cdot \text{sign}(\dot{x}) \end{cases} \quad (10)$$

In the rest of the paper we focus on a two-twin-sensor site layout where both acoustic and magnetic parameters are available. The geometry is shown on figure 7: the source velocity is 10m/s, CPAs are respectively 1000m and 1500m away from sensors, the distance between both sites is 707m, the center frequency is 200Hz. Standard deviations are also kept unchanged for the rest of the paper and are set to $\sigma_{k,(E/V)1}=1.0$, $\sigma_{k,(D/V)1}=0.5$ for $t_k > 500$, $\sigma_{k,(E/V)2}=1.2$, $\sigma_{k,(D/V)2}=0.6$ for $t_k > 550$, $\sigma_{j1}=0.05$ and $\sigma_{j2}=0.06$ (International System of units).

With these parameters Cramèr Rao Lower Bounds are presented on figure 6. First derivative discontinuities of the light gray curves correspond to the introduction of magnetic parameters at CPAs and disclose a great interest for this kind of association.

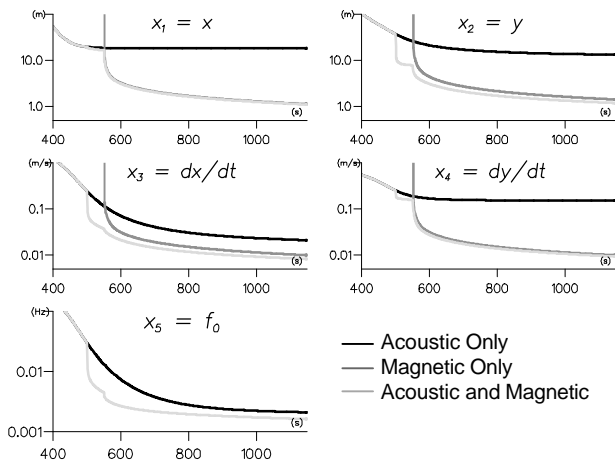


Figure 6. CRLB for two measurement site layout. The first CPA is reached at 500sec while the second is reached at 550sec.

4.3. Monte-Carlo simulations

500 Monte-Carlo simulations were conducted with the same parameters. Results are presented in Table 2 and are compared with acoustic only (AO) and magnetic only (MO) CRLB.

Table 2. Comparison after 1500sec of several CRLB with Monte-Carlo simulation.

| | \mathbf{x}_{true} | $\hat{\mathbf{x}} - \mathbf{x}_{true}$ | σ_{AO} | σ_{MO} | σ_{CRLB} | σ |
|------------|---------------------|--|----------------------|----------------------|----------------------|----------------------|
| x_{tref} | 0.0 | $-2.81 \cdot 10^{-2}$ | 17.946 | 1.120 | 1.092 | 1.269 |
| y_{tref} | -1000. | $-1.44 \cdot 10^{-2}$ | 13.074 | 1.405 | 1.179 | 0.895 |
| \dot{x} | 10. | $1.64 \cdot 10^{-4}$ | $2.10 \cdot 10^{-2}$ | $9.92 \cdot 10^{-3}$ | $8.21 \cdot 10^{-3}$ | $7.95 \cdot 10^{-3}$ |
| \dot{y} | 0. | $-6.10 \cdot 10^{-5}$ | $1.51 \cdot 10^{-1}$ | $9.92 \cdot 10^{-3}$ | $9.32 \cdot 10^{-3}$ | $9.38 \cdot 10^{-3}$ |
| f_0 | 200. | $1.30 \cdot 10^{-4}$ | $2.12 \cdot 10^{-3}$ | XX | $1.63 \cdot 10^{-3}$ | $1.17 \cdot 10^{-3}$ |

Finally, we present on figure 7 the source localization as well as two-sigma uncertainty ellipses. Most information of acoustic measurements delivered around the CPA, as the Doppler frequency rate-of-change is maximum: acoustic only CRLB before and after the first CPA are thus strongly improved and localization estimates are shown to lay inside constant angular sector starting at the last CPA.

Addition of magnetostatic parameters is shown to improve localization estimates of one order of magnitude. Far from the last CPA the positioning accuracy is kept high in this simulation but in the real world bias are often observed directly in the measured parameters E/V and D/V .

5. CONCLUSION

In this paper we have shown interesting results dealing with the association of narrow band acoustic signals and magnetostatic measurements. If only few sensors are available, magnetostatic sites improve positioning accuracy while acoustic parameters improve identifiability. This method was successfully tested on real magnetic

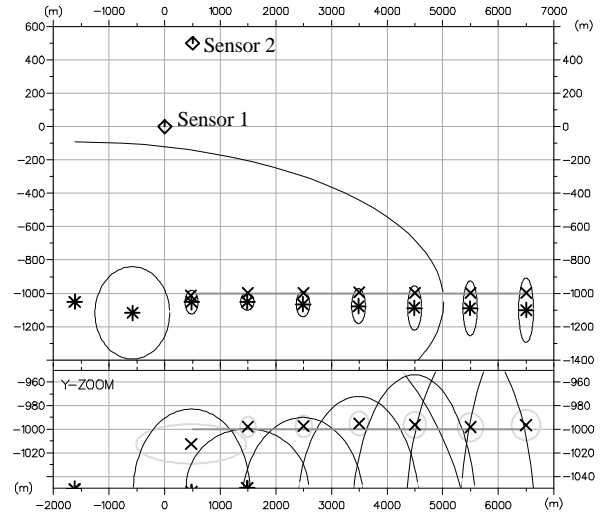


Figure 7. Source localization and two-sigma uncertainty ellipses. It should be strongly emphasize that both axis of each ellipse are scaled identically by the Y-scale. Asterisks (resp. crosses) represent outputs of the Maximum Likelihood estimator strictly based on the past history of acoustic only measurements (resp. of both acoustic and magnetic measurements).

signals and we are currently working on an experimentation involving mixed measurements.

REFERENCES

- [1] G. Dassot, R. Blanpain, "Data Association from two Acoustic-Magnetic Measurement Sites", IEEE Workshop on DSP, Loen, Norvege, 1996.
- [2] C. Jauffret, D. Bouchet, "Frequency Line Tracking on a Lofagram: an Efficient Wedding between Probabilistic Data Association Modelling and Dynamic Programming Techniques", Asilomar Conf., Monterey, USA, 1996.
- [3] R. Blanpain, "Traitement en temps réel du signal issu d'une sonde magnétométrique pour la détection d'anomalies magnétiques", Thèse de l'I.N.P.G., 1979.
- [4] Y. Caritu, "Détection, localisation d'un mobile ferromagnétique dans un réseau de magnétomètres scalaires", Thèse de l'I.N.P.G., 1996.
- [5] J.F. Arnold, Y. Bar-Shalom, R. Estrada, R.A. Mucci, "Target Parameter Estimation Using Measurements Acquired with a Small Number of Sensors", IEEE J. Ocean. Eng., Vol. OE-8, No.3, 1983.